

**PAPER**

# An Imaging Algorithm of a Target with Arbitrary Motion for Ultra Wide-Band Radar with a Small Number of Antennas

**Yuji MATSUKI<sup>†a)</sup>, Student Member, Takuya SAKAMOTO<sup>†</sup>, Member, and Toru SATO<sup>†</sup>, Fellow**

**SUMMARY** UWB (ultra wide-band) pulse radar is a promising candidate for surveillance systems. The fast SEABED (Shape Estimation Algorithm based on BST and Extraction of Directly scattered waves) imaging algorithm is deployed in the application of UWB pulse radar in fields that require real-time operations. However, since the SEABED algorithm uses signals received at multiple locations, this method either needs to scan antennas or to install many antennas. Such systems are inevitably costly and unrealistic for applications such as surveillance. To overcome this problem, a revised SEABED algorithm that estimates unknown target shape based on target motion using only a pair of fixed antennas was developed. However, the method cannot be used when the target moves arbitrarily because it assumes the target motion is parallel to the baseline of the pair of antennas. In this paper, we propose a new UWB radar imaging algorithm that is applicable even for targets with arbitrary motion. The proposed method introduces another antenna which is added to the pair of antennas used in the revised SEABED, and estimates unknown target motion based on the target surface using the three antennas. Next, the proposed method applies the SEABED imaging algorithm to the estimated motion and obtains the target image. Some numerical simulations establishes that the proposed method can accurately estimate the target shape even under severe conditions.

**key words:** ultra wide-band, pulse radar, shape estimation, moving target

## 1. Introduction

In recent years, developing a reliable surveillance system has been a major issue in crime prevention. Although cameras have been universally prevalent as devices for security systems, they have drawbacks, such as difficulty in accurately estimating the three-dimensional shape of a target, and the exact distance to a target [1], [2]. In addition, they cannot establish the target shape in dark or smoky locations.

Using radar systems is an efficient approach to solving these problems of camera-based conventional systems. UWB (ultra wide-band) radar in particular, is a powerful tool for this purpose because of its three-dimensional imaging capability with exceptionally high resolution. A variety of algorithms have been proposed for imaging using UWB radar systems [3]–[5]. However, these conventional imaging methods are based on iterative procedures that require unrealistically intensive computation for application in surveillance systems. To address these issues, we have developed the SEABED imaging algorithm [6]–[8], which has been deployed to apply UWB pulse radar in fields that require

real-time operations such as surveillance. The SEABED algorithm assumes a system with a scanning antenna or array antennas and fixed targets. However, this type of system is high-cost and unrealistic for use in applications such as a surveillance system. To avoid the use of antenna systems, a revised SEABED method [9], [10] has been developed, which makes use of the motion of the target, such as a human body, instead of antenna scanning as in the case of previous studies. The revised SEABED algorithm requires only a pair of fixed antennas to estimate the motion and shape of a target that moves through the radar system. However, this method cannot be applied to arbitrary motion of the target, since it assumes that the target moves in a line parallel to the antenna baseline, a condition that is critical for application in a real environment.

We propose a new UWB radar imaging algorithm that is applicable even for targets with arbitrary motion, by extending the revised SEABED algorithm. First, we explain the procedure of the proposed method and show an application example and an image obtained for a target with arbitrary motion. Next, we clarify the performance limits of the method under various conditions to show that the proposed method is robust and performs well for a variety of motion types, target shapes, signal-to-noise ratio values, and antenna intervals.

## 2. System Model

The system model in this paper is shown in Fig. 1. For simplicity, we deal with two-dimensional problems in this paper. A target is assumed to be a human body, and the objective is to estimate the shape of the target. We use three omnidirectional antennas spaced at intervals of  $X_0$ . The positions of the antennas #1, #2, and #3 are defined as  $(-X_0, 0)$ ,  $(0, 0)$ , and  $(X_0, 0)$ . We measure the distance from each antenna to a scattering object, and obtain  $R_1(t)$ ,  $R_2(t)$ , and  $R_3(t)$  for antennas #1, #2, and #3. Each measurement is independent of the positions of the other antennas in the system, which implies three mono-static radar systems. We assume that the radar signals do not interfere with each other, and the target motion  $\mathbf{X}(t) = (X(t), Y(t))$  is an unknown function of time  $t$ . We assume a monocycle pulse with a center frequency of 6.0 GHz as a transmit pulse waveform.

## 3. Conventional Imaging Method

SEABED is a fast radar imaging algorithm developed in pre-

Manuscript received May 11, 2010.

Manuscript revised November 15, 2010.

<sup>†</sup>The authors are with the Department of Communications and Computer Engineering, Graduate School of Informatics, Kyoto University, Kyoto-shi, 606-8501 Japan.

a) E-mail: kyoto.yuuji@technology05.mbox.media.kyoto-u.ac.jp

DOI: 10.1587/transcom.E94.B.742

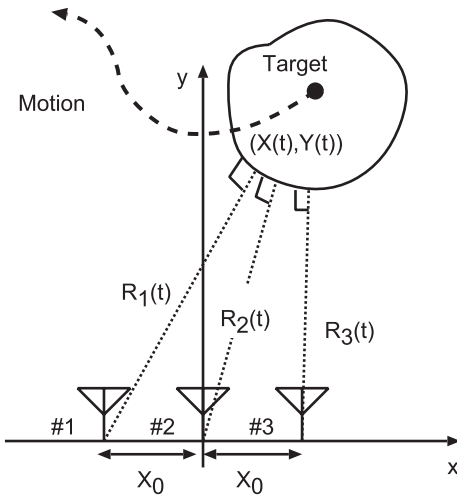


Fig. 1 Two-dimensional system model.

vious work [6]–[8], which is applicable to the system described above only if  $Y(t)$  is constant and  $X(t)$  is known. The algorithm is based on a reversible transform BST (boundary scattering transform) and IBST (inverse BST) between the target shape and received signal, which requires only one of the three antennas assumed in the previous section. Here we define  $R(t) = R_2(t)$ , although we could equally have used  $R_1(t)$  or  $R_3(t)$ . With the range  $R(t)$ , the  $x$ -coordinate of the location of antenna  $X(t)$ , and the scattering center  $(x(t), y(t))$  the following equations of the IBST are satisfied as

$$\begin{cases} x(t) = -X(t) + R(t) \frac{dR(t)}{dX(t)}, \\ y(t) = R(t) \sqrt{1 - \left(\frac{dR(t)}{dX(t)}\right)^2}. \end{cases} \quad (1)$$

Because this IBST requires  $X(t)$ , the location of the target at time  $t$ , the SEABED algorithm cannot be used for imaging unless the movement of the target is known.

To remove the limitation of the SEABED algorithm, a revised algorithm has been proposed [9], [10], which employs a pair of antennas to estimate the target motion  $X(t)$  under the condition  $Y(t) = \text{const}$ . Note that it is difficult to directly estimate the target location using a triangulation technique, because the scattering center moves along the target surface as depicted in Fig. 2. This figure shows that the motion of the scattering centers cannot be ignored for a near target of a certain size, as numerically confirmed in the previous work [10]. It is thus imperative to distinguish between the motion of the target itself and the motion of a scattering center along the surface. For example, let the pair of antennas be  $R_1(t)$  and  $R_2(t)$ . The revised SEABED algorithm finds a continuous function  $\tau(t)$  that satisfies

$$Y_1(\tau(t)) = Y_2(t), \quad (2)$$

and then the target motion  $X(t)$  is estimated as

$$X(t) \simeq \int \frac{2X_0}{\tau(t) - \tau^{-1}(t)} dt. \quad (3)$$

Now imaging can be done with the SEABED algorithm us-

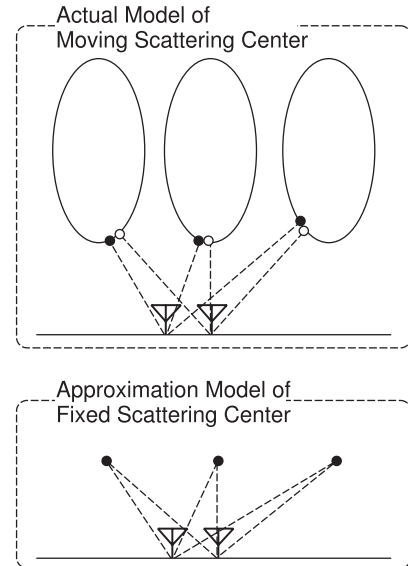


Fig. 2 Actual motion of scattering centers and an approximation with a point-line target.

ing the estimated  $X(t)$  in Eq. (3). Although the effectiveness of the revised SEABED algorithm has been verified [9], [10], the condition  $Y(t) = \text{const}$ . still applies, which is not realistic in practice.

#### 4. Proposed Imaging Method

Conventional methods enforce the unrealistic condition  $Y(t) = \text{const}$ . In this section, we propose a new imaging method that deals with arbitrary target motion  $X(t) = (X(t), Y(t))$ , and uses three antennas as is the case in our system model. First, the proposed method estimates an approximate center  $c(t) = (c_x(t), c_y(t))$  and radius  $a(t)$  of the curvature using  $R_1(t)$ ,  $R_2(t)$ , and  $R_3(t)$  obtained by solving

$$\begin{cases} R_1(t) = \sqrt{(c_x(t) + X_0)^2 + (c_y(t))^2} - a(t), \\ R_2(t) = \sqrt{(c_x(t))^2 + (c_y(t))^2} - a(t), \\ R_3(t) = \sqrt{(c_x(t) - X_0)^2 + (c_y(t))^2} - a(t). \end{cases} \quad (4)$$

Figure 3 shows these relationships. Note that the motion of  $c(t)$  includes not only the target motion  $X(t)$ , but also the relative motion of a scattering center  $(x(t) - X(t), y(t) - Y(t))$  along the target surface. Therefore,  $(c_x(t), c_y(t))$  cannot be used as an estimation of target motion.

To overcome this difficulty, the proposed method calculates an average radius of the curvature between two adjacent time steps. When  $t_n$  is defined as the  $n$ -th sampling time and the IPP (inter-pulse period) as  $\Delta t$ , the proposed method calculates the average radius of curvature with  $a(t_n)$  and  $a(t_{n+1})$  as  $\bar{a}(t_{n+\frac{1}{2}}) = (a(t_n) + a(t_{n+1})) / 2$ . Then,  $c(t_n)$  and  $c(t_{n+1})$  are recalculated as  $\bar{c}(t_n)$  and  $\bar{c}(t_{n+1})$ , under the condition that the radius of the curvature is equal to  $\bar{a}(t_{n+\frac{1}{2}})$  when applying LMS (Least Mean Square) criteria. An instantaneous velocity vector  $v_{n+\frac{1}{2}}$  is defined as

$$v_{n+\frac{1}{2}} = (\bar{c}(t_{n+1}) - \bar{c}(t_n)) / \Delta t. \quad (5)$$

This operation effectively separates the target motion  $X(t)$  from the relative motion of a scattering center  $(x(t) - X(t), y(t) - Y(t))$  since the motion of a scattering center dominates the effect of the curvature  $a(t)$  on the radius. In addition, the radius of the curvature  $a(t)$ , in conjunction with the target motion  $X(t)$ , has a significant effect on the center of the curvature  $c(t)$ . This procedure is illustrated graphically in Fig. 4, in which the three circles of curvature at  $t = t_n, t_{n+1}, t_{n+2}$  are depicted with dashed lines. The averaged circles of curvature using adjacent pairs  $t = t_n, t_{n+1}$  and  $t_{n+1}, t_{n+2}$  are shown as solid lines. Each velocity vector is represented by an arrow from the center of one averaged circle to another.

Next, we combine the instantaneous velocity vector with a summation of the form

$$\bar{X}(t_{N+\frac{1}{2}}) = \sum_{n=1}^N \mathbf{v}_{n+\frac{1}{2}} \Delta t \quad (6)$$

to obtain the estimation of the target location  $\bar{X}(t)$ . Note that the initial value  $X(0)$  does not have any effect on the imaging results because it affects only the location of the estimated image. Using this estimated target motion  $\bar{X}(t)$ , the SEABED can now be applied to realize imaging even in the case of arbitrary target motion.

Finally, we eliminate artifacts to obtain the final image. Since most artifacts are scattered and isolated from others,

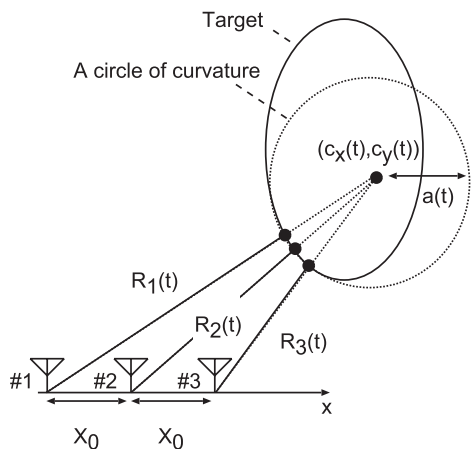


**Fig. 3** Parameters of a circle of curvature.

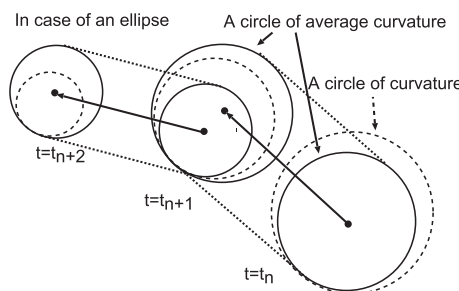


**Fig. 4** Schematic of the averaging circles of curvature in the proposed method.

they can be detected by checking if they have other points in their  $\Delta d$  neighborhood. The method eliminates the  $i$ -th estimated point  $x_i$  if the following condition is satisfied

$$\min_j |x_i - x_j| > \Delta d \quad (i \neq j). \quad (7)$$

where the threshold  $\Delta d$  is determined empirically.

## 5. Performance Evaluation of the Proposed Method

In this section, we validate the performance of the proposed imaging method by means of numerical simulations. The assumed calculation parameters for the simulations are described below. The target shape is assumed to be a slant ellipse with a major axis of 0.25 m and minor axis of 0.15 m as in Fig. 5. This represents an approximated size of a section of the human body. The antenna interval is  $X_0 = 0.5$  m, while the assumed IPP  $\Delta t = 5$  msec. Target motion is given as  $(X(t), Y(t)) = (v_x t, y_0 + y_f \sin \omega t)$ , where  $v_x = -1.0$  m/sec,  $y_0 = 2.0$  m,  $y_f = 0.5$  m and  $\omega = \pi/2$  rad/sec. This motion model is used to investigate the performance of the proposed method for a realistic system model which includes the variation of  $Y(t)$ ; while the revised SEABED algorithm [10] assumes only a simple case with  $Y(t) = \text{const.}$ . The typical walking motion of a human is obviously more likely to be in a straight line. Data obtained under these conditions for  $-2 \leq t \leq 2$  sec are shown in Fig. 6. For simplicity, we

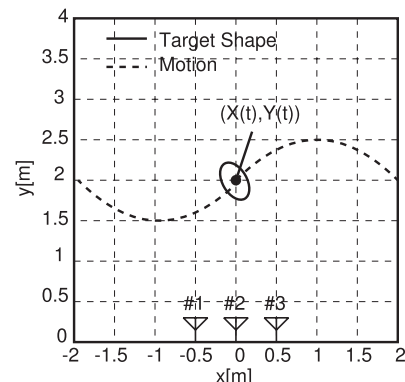


**Fig. 5** Assumed system model for the numerical simulation.

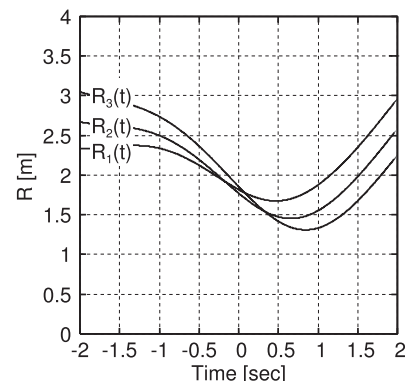


**Fig. 6** Received data  $R_1(t)$ ,  $R_2(t)$  and  $R_3(t)$ .

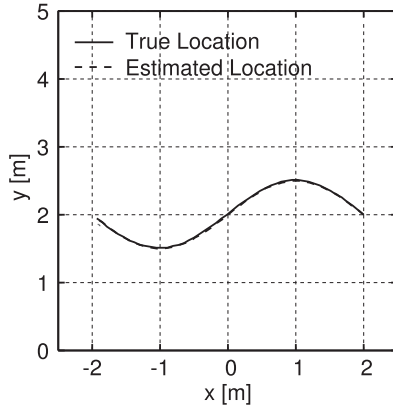


Fig. 7 Target motion estimated using the proposed method.

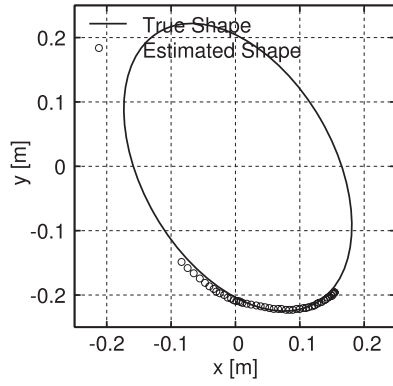


Fig. 8 Target shape estimated using the proposed method.

assume ideal conditions without noise. We set the threshold  $\Delta d$  to 5 mm throughout this paper.

Figure 7 shows the estimated target motion produced by the proposed algorithm. The actual and estimated motion curves overlap almost entirely, indicating that the accuracy of the estimation is quite high. Figure 8 shows the target shape estimated using the proposed algorithm. Here, the error  $e_i (i = 1, 2, 3, \dots, n)$  is defined as the distance between each estimated point and the closest point on the actual target surface as:

$$e_i = \min_{\mathbf{p}} |\mathbf{x}_i - \mathbf{p}|, \quad (8)$$

where  $\mathbf{p}$  is a point on the actual target surface and  $\mathbf{x}_i$  is the  $i$ -th estimated point. In this paper, the RMS error  $\epsilon = \sqrt{\sum e_i^2/n}$  is defined to evaluate the accuracy of the estimated shape using the proposed method. The RMS error  $\epsilon$  in Fig. 8 is about 4.0 mm, which corresponds to 1.6% of the major axis and 2.7% of the minor axis of the assumed target shape.

## 6. Evaluation of the Proposed Method under Other Conditions

In this section, we apply the proposed method to a moving

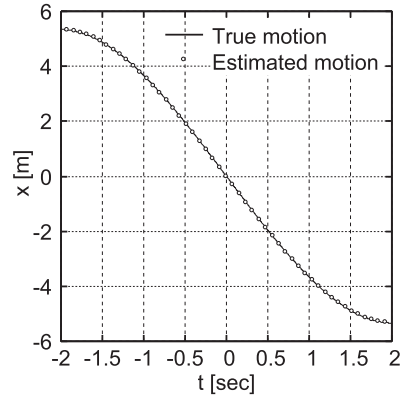


Fig. 9 Actual target motion and estimation using the proposed method.

target under various conditions, and investigate the performance limits of the method using numerical simulation. The calculation parameters for the simulations are as follows: a target shape is assumed to be an ellipse with a long axis of  $B$  and a short axis of  $W$ , and the distance between antennas is  $X_0$ . In order to simplify a condition, the target ellipse major axis and  $y$  axis are parallel.

### 6.1 Examination of the Proposed Method When Applied to Various Target Motions

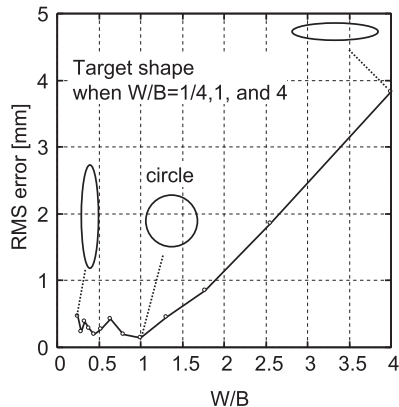
We assume a target motion under acceleration in the X-Y plane ( $X(t), Y(t)$ ) along a straight line at  $Y(t) = 2.0$  m and  $X(t)$  as in Fig. 9. The target speed changes within a realistic range from 0 m/sec to 4 m/sec in 4 sec. We assume that  $X_0 = 0.5$  m,  $B = 0.25$  m,  $W = 0.15$  m.

Figure 9 shows the target motion estimated by the proposed algorithm. The actual and estimated curves overlap almost entirely, meaning that the motion estimation process works well for this example. The RMS error  $\epsilon$  between the estimated and true target shapes is approximately 0.63 mm, which corresponds to 0.25% and 0.42% of the long and short axes of the target shape. Thus it is established that the proposed method can accurately estimate the motion and shape of a target even if the motion involves a large acceleration.

### 6.2 Examination of the Proposed Method When Applied to Various Target Shapes

Next, we investigate the accuracy of the proposed method for estimating different target shapes. We change the target shape by changing the ratio  $W/B$  between the long axis  $B$  and short axis  $W$  of an ellipse. Here, the cross-sectional area of the target is fixed at  $0.04\pi\text{m}^2$ . The target motion is  $(X(t), Y(t)) = (v_x t, y_0)$ , where  $v_x = -1.0$  m/sec,  $y_0 = 2.0$  m, and  $X_0 = 0.5$  m.

We see that the RMS error  $\epsilon$  between the estimated and true target shapes becomes relatively large for large  $W/B$  in Fig. 10. This is because of the difference in curvatures. The radius of the curvature around the scattering centers becomes large when  $W/B$  is large. Consequently, the three



**Fig. 10** RMS error between the estimated and true target shapes versus the ratio of the long and short axis of the target.

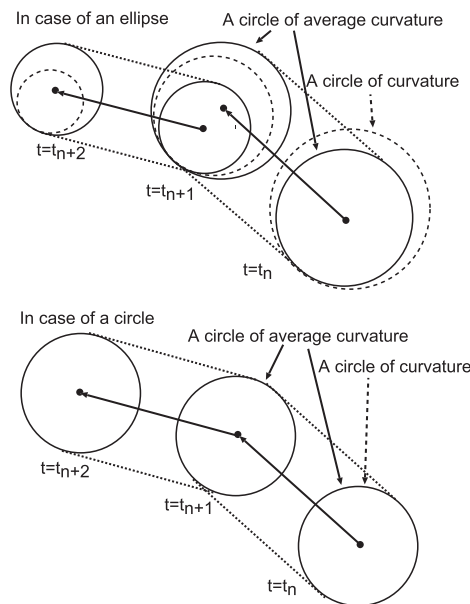


**Fig. 11** Accuracy of estimation with approximation processes for an ellipse and a circle target.

scattering centers separate from each other, reducing the accuracy of estimating curvatures using the proposed method, because we estimate the circle of curvature by estimating a circle on which three scattering centers are located. In contrast, the RMS error  $\epsilon$  becomes relatively small for small  $W/B$ . This is because the three scattering centers are located close together in this case, making the circular model a good approximation of the local target shape.

The RMS error  $\epsilon$  is the smallest for  $B = W$  as in Fig. 10. This is because the target shape is a complete circle in this situation, and the approximation process using a curvature circle is not an approximation but a direct expression of the target shape in this case. As in the upper figure of Fig. 11, if the target shape is an ellipse, this approximation has a certain error, requiring the averaging of two adjacent curvatures. In contrast, the curvature averaging process is not needed at all if target shape is a circle as in the lower figure

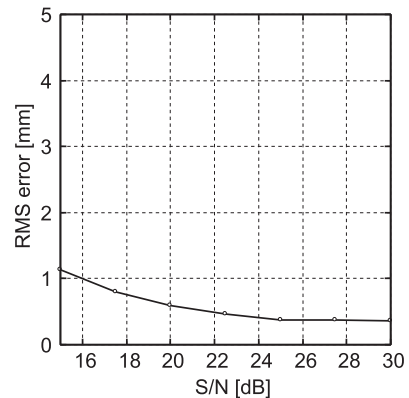


**Fig. 12** RMS error between the estimated and true target shapes versus the S/N obtained in noisy circumstances.

of Fig. 11.

### 6.3 Examination of the Noise Tolerance of the Proposed Method

In this section, we investigate the imaging performances of the proposed algorithm in noisy situations. We add Gaussian error to the  $R_1(t)$ ,  $R_2(t)$ , and  $R_3(t)$ , which is an approximation of added white Gaussian noise included in the received signals. A relationship between the signal-to-noise ratio (S/N) and the standard deviation of the Gaussian random error in measured distance is shown in [7]. Here, the S/N is defined as a ratio of peak instantaneous signal power to the averaged noise power after applying a matched filter. In this section, we assume the S/N is always larger than 15 dB while the S/N depends on the distance between the scattering center object and an antenna. We add the noise to  $R_1(t)$ ,  $R_2(t)$ , and  $R_3(t)$ , and smooth them with a Gaussian function with a correlation length of 1 cm. Target motion is  $(X(t), Y(t)) = (v_x t, y_0)$ , where  $v_x = -1.0 \text{ m/sec}$ ,  $y_0 = 2.0 \text{ m}$ . We assume that  $B = 0.25 \text{ m}$ ,  $W = 0.15 \text{ m}$ , and  $X_0 = 0.5 \text{ m}$ .

Even with added noise, accurate imaging is realized by the proposed method as shown in Fig. 12. However, it is noted that the number of estimated points decreases for lower S/N. This is because the lower S/N increases the number of false image points which do not include other estimated points within 5 mm and we eliminate these points in this paper.

### 6.4 Examination of the Influence of an Antenna Interval

Finally, we investigate the performance of the proposed method with different antenna intervals. The target motion is given as  $(X(t), Y(t)) = (v_x t, y_0)$ , where  $v_x = -1.0 \text{ m/sec}$ ,  $y_0 = 2.0 \text{ m}$ . We assume  $B = 0.25 \text{ m}$  and  $W = 0.15 \text{ m}$ . We add Gaussian noise to  $R_1(t)$ ,  $R_2(t)$ , and  $R_3(t)$  with an S/N of 15 dB and we smooth them by collapsing a Gaussian function, where  $\sigma = 0.01$ .

The RMS error  $\epsilon$  between the estimated and true target shapes becomes very large when the antenna interval is

smaller than 0.2 m as in Fig. 13. This is because the parameters of the calculated circle of curvature have unstable values. When the antenna interval is short,  $R_1(t)$ ,  $R_2(t)$ , and  $R_3(t)$  are almost the same. Therefore, the parameters of the circle of curvature are changed sharply by slight noises. For this reason, motion and shape estimation by the proposed method has a large error in this situation.

We see that the RMS error  $\epsilon$  becomes relatively large for large  $X_0$  as shown in Fig. 13. The proposed method approximates the local shape of a target using a circle, which requires the scattering center points are close enough. However, this assumption does not hold for a large antenna interval  $X_0$  because the distance between scattering centers becomes large when the antennas are located far from each other as shown in Fig. 14. The upper and lower figures in

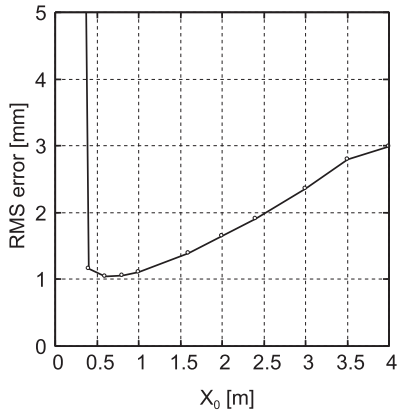


Fig. 13 RMS error between the estimated and true target shapes versus the antenna distance  $X_0$ .

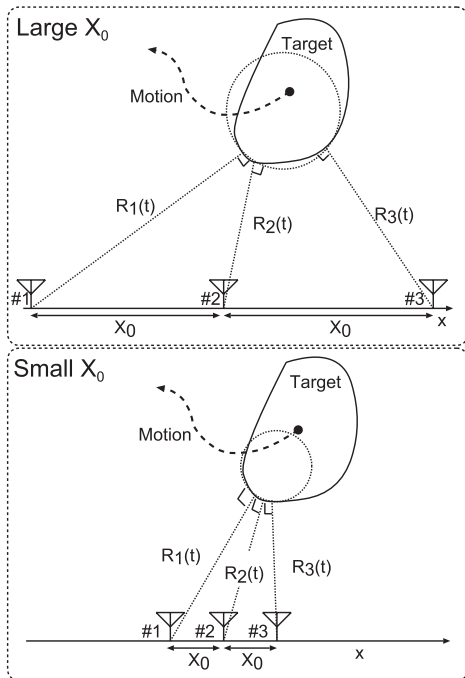


Fig. 14 Examples of circles of curvature for large and small  $X_0$ .

Fig. 14 show examples of scattering centers for the large and small  $X_0$ .

## 7. Performance Comparison with the Conventional Method

Next, we verify the performance limitations of the revised SEABED algorithm [10] that does not satisfy the condition  $Y(t) \neq \text{const.}$  with respect to target motion. For simplicity, we assume uniform motion along a straight line with an inclination angle  $\theta$  to the antenna baseline. The RMS error  $\epsilon$  between the estimated and true target shapes using the revised SEABED algorithm is shown in Fig. 15. Here, we assume a slant ellipse with a long axis of 0.25 m and a short axis of 0.15 m, and the antenna interval is 0.5 m. The assumed model for the revised SEABED algorithm corresponds to  $\theta = 0^\circ$ , where the RMS error  $\epsilon$  is sufficiently small, thereby indicating that an accurate imaging can be realized. The RMS error  $\epsilon$ , however, is relatively large even for  $0^\circ < \theta \leq 10^\circ$ .

In contrast, the RMS error  $\epsilon$  of the shape estimation using the proposed method under the same conditions is shown in Fig. 16. This result confirms that the proposed method es-

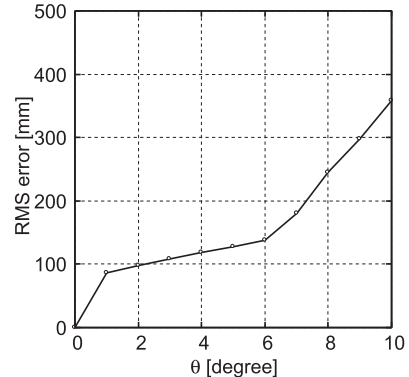


Fig. 15 RMS error between the estimated and true target shapes using the revised SEABED algorithm with an inclination angle  $\theta$  for target motion along a straight line.

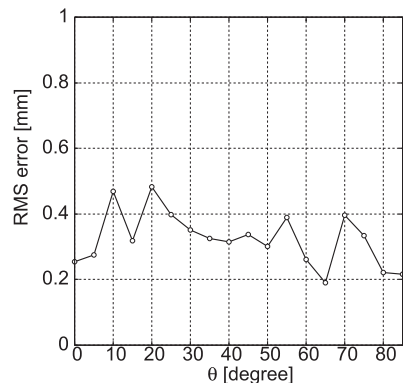


Fig. 16 RMS error between the estimated and true target shapes using the proposed method with an inclination angle  $\theta$  for target motion along a straight line.

timates the target shape accurately for  $0^\circ \leq \theta \leq 85^\circ$ . Note that the proposed method cannot be applied for  $\theta = 90^\circ$  because the SEABED assumes that the relative motion of a target has a component in the cross-range direction, which is not satisfied for  $\theta = 90^\circ$ .

## 8. Discussion

### 8.1 The Necessity for Three Antennas

First, we clarify why three antennas are necessary for the proposed method. If only two antennas #1 and #2 were used, all the observed data would be either  $R_1(t)$  or  $R_2(t)$ . In general, the locations of the scattering centers for these antennas are different, as illustrated in Fig. 2. However, when a point-like target is assumed, the location can be uniquely determined with  $R_1(t)$  and  $R_2(t)$  and the antenna interval  $X_0$  using a triangulation technique. In other words, these two cases cannot be distinguished if only two antennas are used. Therefore, the use of three antennas is a necessary condition for imaging a target with arbitrary motion. In this paper, we showed that our proposed method can estimate arbitrary motion with three antennas. This implies that the use of three antennas is a sufficient condition for this problem.

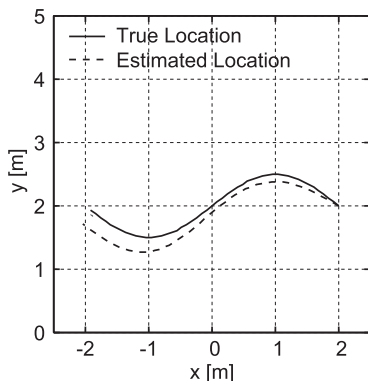


Fig. 17 Locus of the center of curvature.

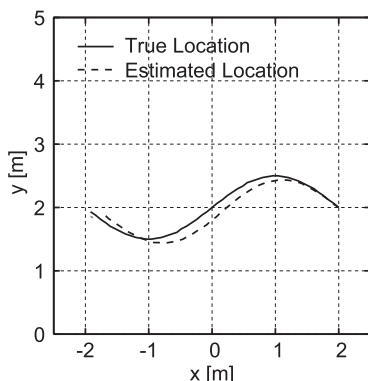


Fig. 18 Locus of the estimated scattering center.

### 8.2 The Motion Estimation by Other Methods

Next, we discuss why the averaging of two radii is necessary. One might assume that the center of curvature or the estimated scattering center could be used as an estimation of target motion  $X(t)$ . In fact, neither of these values can be used for this estimation. Figure 17 and Fig. 18 show the loci of the center of curvature  $c(t)$  and the scattering center estimated by assuming a point-like target. The assumed model is the same as in the previous section. Both results show that such simple methods cannot be used to estimate target motion, since these methods are not able to separate the motion of a target from the motion of a scattering center.

## 9. Conclusions

In this paper, we proposed a new UWB radar imaging method. Conventional methods [10] cannot estimate the shape of a target that moves arbitrarily, because the method assumes the target motion is parallel to the baseline of a pair of antennas. In contrast, although the proposed method requires an additional antenna, using three antennas in total, it provides an accurate estimation of target motion and shapes for arbitrary motion. We verified that the proposed method realizes accurate imaging under various conditions, and established the application limits of the method using the RMS error  $\epsilon$  of the differences between the actual and estimated shapes. Even if the target motion accelerates, it has been verified that the proposed method can estimate the target motion and shape with high accuracy, and that the RMS error  $\epsilon$  is 0.63 mm for the motions assumed in this study. Moreover, the proposed method can accurately estimate a target shape with a relatively large curvature, or a target shape close to a circle. The RMS error  $\epsilon$  is 0.46 mm and 3.8 mm for  $W/B = 1/4$  and  $W/B = 4$ , and reaches a minimum of 0.14 mm for  $W = B$ . In noisy environments, the RMS error  $\epsilon$  is 0.36 mm for  $S/N = 30$  dB, while it becomes 1.1 mm for  $S/N = 15$  dB. When the antenna interval is smaller than 0.2 m, the proposed method does not work well because of the influence of noise. The RMS error  $\epsilon$  reaches a minimum of 1.0 mm for an antenna interval of 0.6 m.

## References

- [1] S.H. Seo, M.R.A-Sadjadi, and B. Tian, "A least-squares-based 2-D filtering scheme for stereo image compression," *IEEE Trans. Image Process.*, vol.9, no.11, pp.1967–1972, Nov. 2008.
- [2] V. Lippiello, B. Siciliano, and L. Villani, "Position-based visual servoing in industrial multi-robot cells using a hybrid camera configuration," *IEEE Trans. Robot.*, vol.23, no.1, pp.73–86, Feb. 2007.
- [3] E.J. Bond, X. Li, S.C. Hagness, and B.D. van Veen, "Microwave imaging via space-time beam forming for early detection of breast cancer," *IEEE Trans. Antennas Propag.*, vol.51, no.8, pp.1690–1705, 2003.
- [4] J. van der Kruk, C.P.A. Wapenaar, J.T. Fokkema, and P.M. van den Berg, "Three-dimensional imaging of multi-component ground-penetrating radar data," *Geophysics*, vol.68, no.4, pp.1241–1254, 2003.

- [5] R.M. Narayanan, X. Xu, and J.A. Henning, "Radar penetration imaging using ultra-wideband (UWB) random noise waveforms," IET Proc. Radar Sonar Navig., vol.151, no.3, pp.143–148, 2004.
- [6] T. Sakamoto and T. Sato, "A target shape estimation algorithm for pulse radar systems based on boundary scattering transform," IEICE Trans. Commun., vol.E87-B, no.5, pp.1357–1365, May 2004.
- [7] T. Sakamoto, "A 2-D image stabilization algorithm for UWB pulse radars with fractional boundary scattering transform," IEICE Trans. Commun., vol.E90-B, no.1, pp.131–139, Jan. 2007.
- [8] T. Sakamoto, "A fast algorithm for 3-dimensional imaging with UWB pulse radar systems," IEICE Trans. Commun., vol.E90-B, no.3, pp.636–644, March 2007.
- [9] T. Sakamoto and T. Sato, "Real-time imaging of human bodies with UWB radars using walking motion," 2007 IEEE International Conference on Ultra-Wideband (ICUWB2007), pp.24–26, Singapore, Marina Mandarin Hotel, Sept. 2007.
- [10] T. Sakamoto and T. Sato, "2-Dimensional Imaging for Human Bodies with UWB Radar using Approximately Uniform Walking Motion along a Straight Line with the SEABED Algorithm," IEICE Trans. Commun., vol.E91-B, no.11, pp.3695–3703, Nov. 2008.



**Yuji Matsuki** received the B.E. degree from Kyoto University in 2009. He is currently studying for the M.I. degree at Graduate School of Informatics, Kyoto University. His current research interest is in signal processing for the near field radar, UWB radar. He is a member of the Institute of Electrical and Electronics Engineers (IEEE).



**Takuya Sakamoto** received his B.E. degree from Kyoto University in 2000, and M.I. and Ph.D. degrees from the Graduate School of Informatics, Kyoto University in 2002 and 2005, respectively. He is an assistant professor in the Department of Communications and Computer Engineering, Graduate School of Informatics, Kyoto University. His current research interest is in UWB radar signal processing. He is a member of the IEEJ and the IEEE.



**Toru Sato** received his B.E., M.E., and Ph.D. degrees in electrical engineering from Kyoto University, Kyoto, Japan in 1976, 1978, and 1982, respectively. He has been with Kyoto University since 1983 and is currently a Professor in the Department of Communications and Computer Engineering, Graduate School of Informatics. His major research interests include system design and signal processing aspects of UWB radars, atmospheric radars, radar remote sensing of the atmosphere, and radar observation of space debris. He is a member of the Institute of Electrical and Electronics Engineers, the Society of Geomagnetism and Earth, Planetary and Space Sciences, the Japan Society for Aeronautical and Space Sciences, and American Meteorological Society.